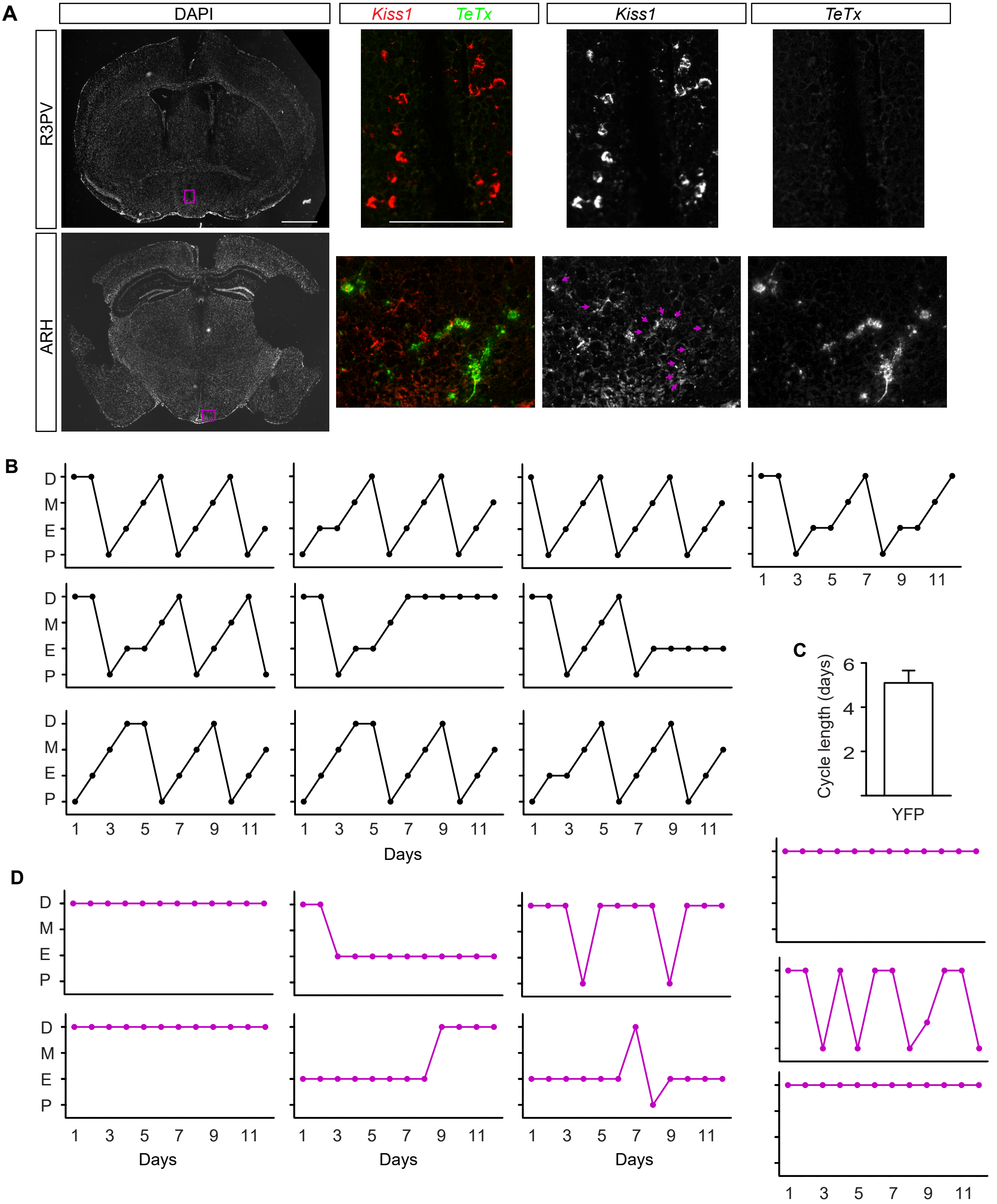

Figure S1. Validation of viral targeting and estrous cycle tracking of Kiss1^{ARH}-silenced mice. Related to Figure 1.
A) Left, DAPI-stained coronal sections of the R3PV (top) and ARH (bottom). Magenta box indicates the area shown to the right. Right, *TeTx* and *Kiss1* transcript expression of a representative Kiss1^{ARH}-silenced mouse. Magenta arrowheads indicate overlap.
B-D) 12-day of estrous cycle tracking in YFP-injected controls (**B**, black) and TeTx-silenced mice (**D**, magenta). Individual mice in each cohort are shown.
C) Average time between proestrus of control mice (avg cycle length = 5.1 day, n = 10, se = 0.56)
Abbreviations: D, diestrus; M, metestrus; E, estrus; P, proestrus. Scale bars; A, left 500 μm; right 100 μm.

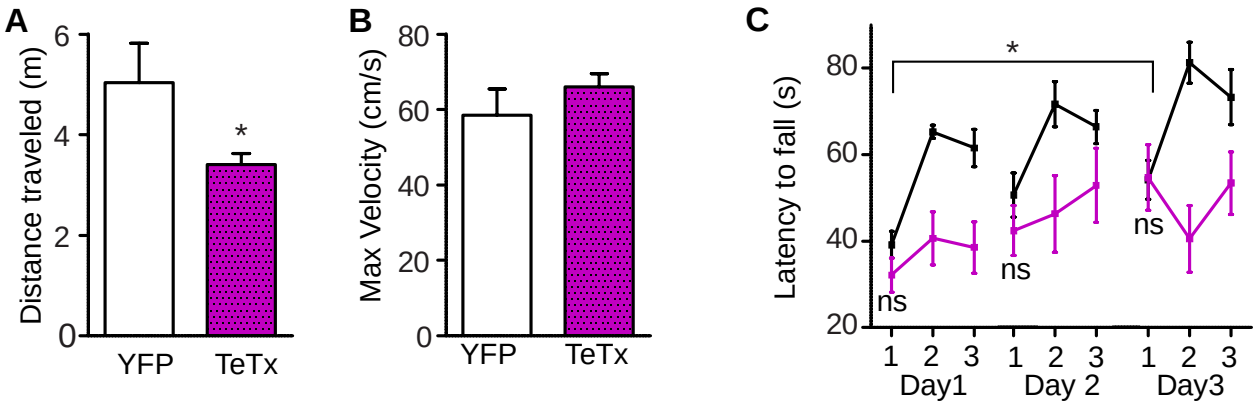

Figure S2. Kiss1^{ARH}-silenced mice have normal motor coordination and can learn a motor task. Related to Figures 1-3.

A and B) Movement tracking in an open field (novel environment) comparing Kiss1^{ARH} silenced (pink) mice with YFP-injected controls (white). (**A**) Distance traveled, Mann-Whitney test: TeTx (n = 8), distance = 3407 ± 600.7 m; YFP (n = 8), distance = 5038 ± 2212 m; p = 0.0499. (**B**) Maximum velocity reached during trial, Student t-test, YFP (n = 8) velocity = 58.50 ± 19.45 cm/s; TeTx (n = 8) velocity = 66.08 ± 9.52 cm/s, $t_{(14)}$ = 0.991, p = 0.339.

C) Motor learning assessed by the latency to fall from a rotating cylinder (2-min trial, ramp 4—40 RPM). Two-way ANOVA of the first test on days 1-3: TeTx (n = 8), YFP (n = 8), $F_{(1,28)}$ = 0.778, p = 0.393. There was a difference between the first trial scores on days 1 vs 3 for both groups; $YFP_{(d1\ vs\ d3)}$, p = 0.016; $TeTx_{(d1\ vs\ d3)}$, p = 0.020

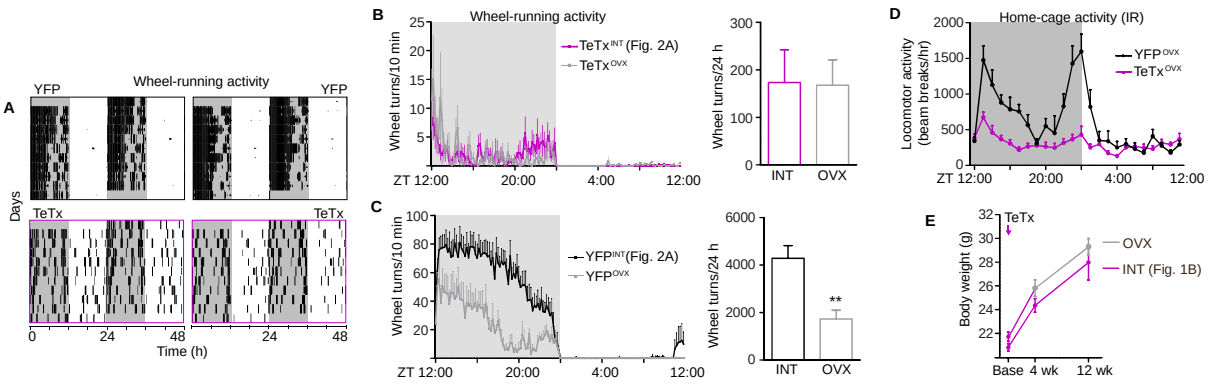

Figure S3. Ovariectomy Does Not Change the Effect of Kiss1^{ARH} Silencing with Respect to Locomotor Activity or Body Weight. Related to Figures 1-3.

A) Representative actograms of running-wheel activity from two mice in each cohort, double plotted. Note, the activity of Kiss1^{ARH}-silenced mice (bottom, purple boxes) was amplified to visualize the pattern of wheel-running activity in a 10-min bin.

B) Waveform of daily running wheel activity comparing intact (pink, shown in Figure 2A) and ovariectomized (grey) Kiss1^{ARH}-silenced mice (3 d average for each mouse). Cumulative 24h wheel activity is shown to the right. Student t-test comparison: TeTx (intact, n = 8), wheel revolutions = 173.6 ± 194.7 turns; TeTx (ovx, n = 8), wheel revolutions = 167.7 ± 151.6 turns, $t_{(14)} = 0.07$, p = 0.95

C) Waveform of daily running wheel activity comparing intact (black, shown in Figure 2A) and ovariectomized (grey) YFP control mice (3 d average for each mouse). Cumulative 24-h wheel activity is shown to the right. Student t-test comparison: YFP (intact, n = 8), wheel revolutions = 4282 ± 1518 turns; YFP (ovx, n = 8), wheel revolutions = 1728 ± 1029 turns, $t_{(14)} = 3.34$, **p = 0.0015

D) Waveform of daily home-cage activity (3 d average for each mouse). Two-way ANOVA: *n* = 8 (YFP-OVX), *n* = 8 (YFP-Int), $F_{(1,1344)} = 97.84$, ***p < 0.0001 (main effect of TeTx).

E) Body weight gain following AAV1-DIO-GFP:TeTx delivery into the ARH of *Kiss1^{Cre}* females. Data shown in Figure 1B is compared to a group of Kiss1^{ARH}-silenced mice (n = 8) that received a surgical ovariectomy 4 wk post neuronal-silencing. Two-way ANOVA: $F_{(1,70)} = 3.29$, p = 0.074 (main effect of TeTx).

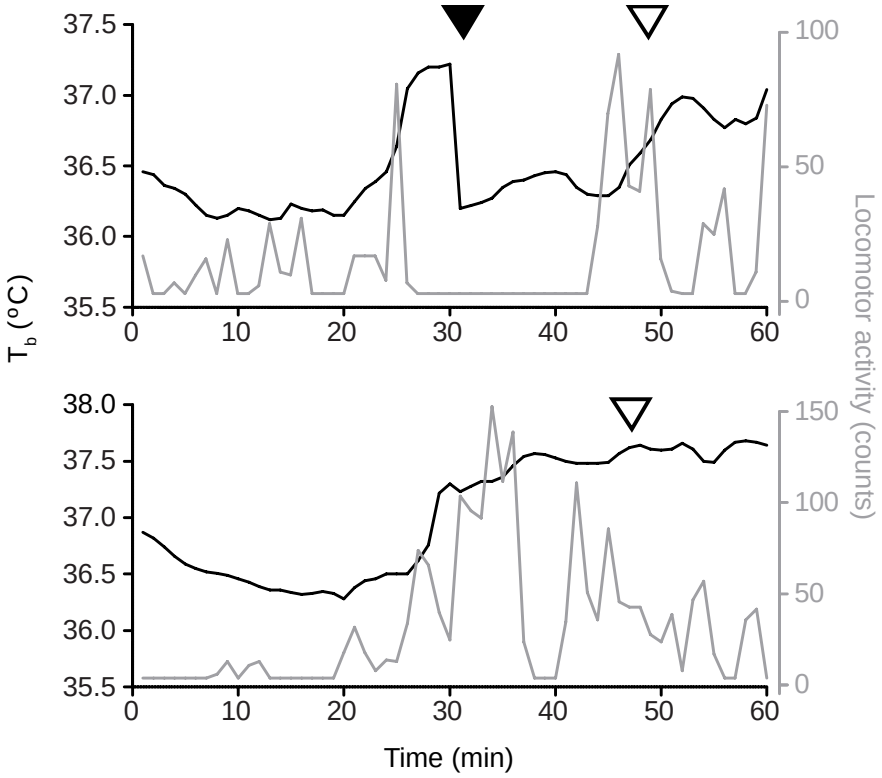

Figure S4. The acute influence of activity on Tb is apparent within 10 min of an activity bout. Related to Figure 4.

Representative traces of Tb and activity at matched time points over a 60-min interval (black trace, Tb; gray trace, activity). Measurements were gathered every minute. Arrowheads indicate Tb fluctuations in response to activity bouts. The solid arrowhead corresponds to an activity bout followed by sustained inactivity, while the open arrowheads indicate Tb in response sustained activity.

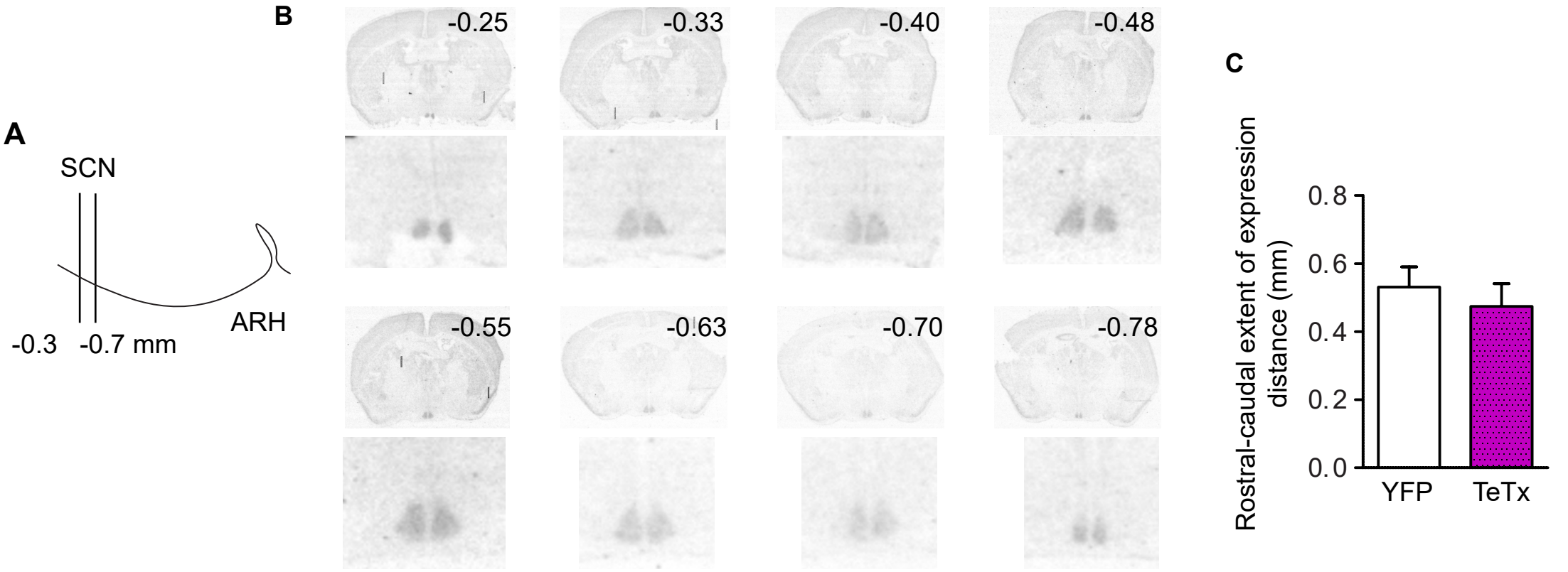

Figure S5. Kiss1^{ARH} Neurons are Not Necessary for the Extent of *Per1* Expression on the Rostral-caudal Axis of the SCN at ZT8. Related to Figure 6.

A) Diagram indicating the rostral-caudal extent of the SCN using Bregma coordinates on a sagittal midline section.
B) Autoradiographic images of serial coronal sections of one representative mouse radiolabeled with a *Per1* probe. Bregma coordinates of the coronal section are indicated. The tissue was prepared at ZT8.
C) Average rostral-caudal length of *Per1* staining in the SCN comparing YFP controls to Kiss1^{ARH}-silenced females.

Student t-test, YFP n = 5, normalized gray scale = 0.47 ± 0.15; TeTxLC n = 8, normalized grey scale = 0.53 ± 0.17, t(11) = 0.62, p = 0.55.

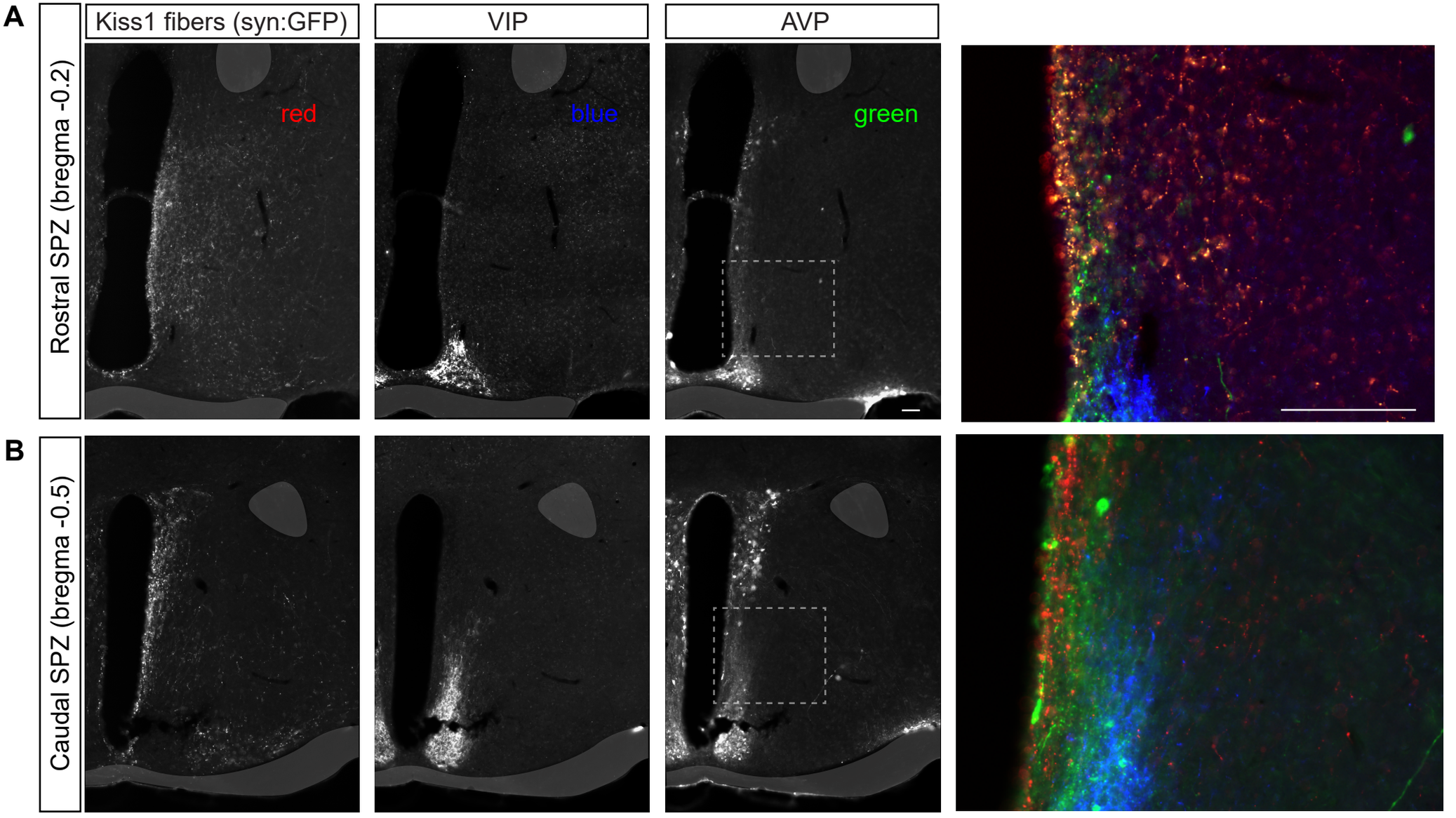

Figure S6. Kiss1^{ARH} Fibers in the SPZ are Intermingled with AVP and VIP Fibers. Related to Figure 6.

AAV-DIO-Syn:GFP was injected into the ARH of *Kiss1^{Cre}* female mice. The coronal sections shown are stained for GFP, VIP and AVP immuno-reactivity.

A) Section containing the rostral SPZ
B) Section containing the caudal SPZ

The colors assigned to each antibody are indicated at the top. The dotted line indicates the segment of area shown in color. Scale bars, 1 mm